



An improved weighted mean temperature (T_m) model based on GPT2w with T_m lapse rate

Fei Yang^{1,2,3} · Jiming Guo^{1,3} · Xiaolin Meng² · Junbo Shi¹ · Di Zhang¹ · Yinzhi Zhao¹

Received: 24 September 2019 / Accepted: 20 January 2020 / Published online: 15 February 2020
© Springer-Verlag GmbH Germany, part of Springer Nature 2020

Abstract

Global pressure and temperature 2 wet (GPT2w) is an empirical model providing the mean values plus annual and semiannual amplitudes of weighted mean temperature (T_m), which makes it a widely used tool in converting zenith wet delay (ZWD) to precipitable water vapor (PWV) in GNSS meteorology. The model meets the needs of real-time T_m anywhere in the world without relying on any other meteorological observations compared with traditional T_m calculation methods. It outperforms the other empirical T_m models released in recent years. Due to the lack of the T_m vertical adjustment in the model, the accuracy of T_m estimated by the model is subject to certain constraints, especially at sites which have large altitude differences compared with the GPT2w grid points. We explored the T_m lapse rate for the vertical adjustment using 10 years of 37 monthly mean pressure level data from the European Center for Medium-Range Weather Forecasts (ECMWF) and extended the GPT2w model to a new one called the GPT2wh model. Three schemes with different height ranges were established to fit the T_m lapse rate, and the most appropriate scheme was selected by adopting the goodness of fit measures, including the coefficient of determination (R -squared) and the root mean square error (RMSE). In addition to the mean value, annual and semiannual amplitudes for T_m lapse rate on a regular 1° grid were determined and stored in the GPT2wh model. The performance of the new model was assessed against the GPT2w model using different data sources in 2011, i.e., the ECMWF data and globally distributed radiosonde data. The numerical results show that the GPT2wh model outperforms the GPT2w model with an improved RMSE of 7.36/5.00/2.45/1.37/0.51/0.03 K at different height levels in the ECMWF comparison. In comparison with the radiosonde data, the mean RMSE of the GPT2wh model improves by 0.33 K from 4.16 to 3.83 K, i.e., an approximately 8% improvement against the GPT2w model. The impact of T_m on GNSS-PWV was analyzed, showing that the GPT2wh model can effectively improve the accuracy of the converted PWV.

Keywords GNSS meteorology · Weighted mean temperature · GPT2w model · ECMWF data · Radiosonde

Introduction

The Global pressure and temperature (GPT) model is an empirical model proposed by Böhm et al. (2007), which is based on spherical harmonics up to degree and order 9 and provides temperature and pressure at any site in the vicinity of the earth's surface. The model is widely used in geodetic

applications, such as reference pressure values for atmospheric loading or the determination of a priori hydrostatic zenith delays.

Lagler et al. (2013) proposed the GPT2 model to improve the limited spatial and temporal variability of the GPT model. GPT2 model provides temperature, pressure, as well as water vapor pressure and mapping function coefficients at any site with a global 5° grid of mean values, alongside annual and semiannual variations in all parameters. This brings forth improved empirical slant delays for geophysical studies.

The global pressure and temperature 2 wet (GPT2w) model is the up-to-date version proposed by Böhm et al. (2015), established on monthly meteorological data of 10-year (2001–2010) ERA-Interim, and developed the weighted mean temperature (T_m) as a new output parameter

✉ Jiming Guo
jimguo@sgg.whu.edu.cn

¹ School of Geodesy and Geomatics, Wuhan University, 129 Luoyu Road, Wuhan 430079, China

² Nottingham Geospatial Institute, The University of Nottingham, Nottingham NG7 2TU, UK

³ Research Center for High Accuracy Location Awareness, Wuhan University, Wuhan 430079, China

with a global resolution of $1^\circ \times 1^\circ$ geographical grid. The T_m is a function of atmospheric temperature and vertical humidity profiles and plays a crucial role in the progress of retrieving water vapor information from the tropospheric delay of GNSS signals (Wang et al. 2005; Sapucci 2014; Wang et al. 2016). The quality of PWV and SWV are affected by the accuracy of T_m (Askne and Nordius 1987; Bevis et al. 1994; Ross and Rosenfeld 1997; Yao et al. 2012).

Traditionally, the T_m can be exactly determined by the atmospheric profiles based on a ray-tracing method, but the atmospheric profiles are almost impossible to obtain in real-time or near real-time at any site. The Bevis formula ($T_m = a + b \cdot T_s$, T_s is the surface temperature) is another alternative, in which the coefficients (a and b) are largely season and location-dependent and should be estimated using meteorological measurements at specific regions and seasons (Bevis et al. 1992; Emardson and Derks 2000; Mendes et al. 2000). It often becomes invalid when in situ temperature measurements are unavailable. To overcome the limitations, some empirical T_m models, fed only by coordinates of the site and the time, have been proposed in recent years, such as the GWMT, GTm-II, GTm-III, GTm_N and GTm_X model (Yao et al. 2012, 2013, 2014; Chen et al. 2014; Chen and Yao 2015). Compared with these empirical models, the GPT2w model is the latest with an excellent performance in T_m calculation verified by scholars (Wang et al. 2016; He et al. 2017; Zhang et al. 2017; Hua et al. 2017; Yang et al. 2019). In addition, the GPT2w model is not a specific T_m model and can output many other atmospheric parameters, making it a widely used tool in meteorology.

In the GPT2w model, it selects the four nearest grid points around the station and calculates their T_m values using the corresponding mean values, annual and semiannual amplitudes from the external grid file. The bilinear algorithm is then adopted to interpolate the T_m of the station from the T_m of the four grid points. However, the grid points of the GPT2w model are not strictly collocated with the GNSS station; therefore, spatial adjustments are always required. In the model, the exponential based on virtual temperature, the temperature lapse rate, and the water vapor decrease factor were applied to fulfill this request for pressure, temperature, and water vapor pressure, respectively (Böhm et al. 2015; Wang et al. 2017). For T_m , however, the model lacks the corresponding parameter for vertical adjustment, which results in inaccuracy in the T_m calculation.

The applications of T_m estimated by this model would be limited because the altitude differences between the GNSS stations and the reference level of the model always exist (Zhang et al. 2017). To solve this issue, the T_m lapse rate along the vertical direction, which can be affected by several factors, (e.g., the atmospheric pressure, moisture content of air and the height), should be considered and applied to the GPT2w model (Yang and Smith 1985; He et al. 2017; Zhang

et al. 2017). We utilized the 10 years (2001–2010) of 37 monthly mean pressure level data from ECMWF to analyze the global T_m lapse rate. The purpose was to determine the mean value as well as annual and semiannual amplitudes for the T_m lapse rate on a regular 1° grid at mean ETOPO5 heights, which is similar to the other parameters of the GPT2w model (Lagler et al. 2013; Böhm et al. 2015). Then, a new model called GPT2wh model was established.

We describe in detail the method of determining the T_m lapse rate in the section of determination of the T_m lapse rate. The mean value as well as annual and semiannual amplitudes for the grid T_m lapse rate is analyzed in the section on analysis of the gridded T_m lapse rate. The GPT2wh model is compared to the GPT2w model using the ECMWF data and the radiosonde data in the section on validation of the T_m lapse rate. Finally, the impact of T_m on GNSS-PWV is analyzed, and the conclusion is given.

Determination of the T_m lapse rate

To explore the vertical dependence of T_m , namely the T_m lapse rate, the T_m profiles of each grid point at a certain moment should be calculated. The T_m can be obtained by numerical integration using the layered meteorological data along the zenith direction, which is expressed as follows (Davis et al. 1985):

$$T_m = \frac{\int \frac{p}{T} dz}{\int \frac{p}{T^2} dz} \quad (1)$$

where T is the atmospheric temperature (in K); p is the partial pressure (in hPa) of water vapor that can be calculated using (Bolton 1980; Wang et al. 2016):

$$P_s = 6.11 \times 10^{\left(\frac{7.5 \times T_d}{237.3 + T_d}\right)} \quad (2)$$

$$p = \frac{rh \times P_s}{100} \quad (3)$$

where P_s is the saturated vapor pressure, rh is the relative humidity, and T_d is the atmospheric temperature (in $^\circ\text{C}$).

To obtain the T_m at each level, we retrieved the 10 years of global monthly mean profiles for temperature, relative humidity, and geopotential from the ERA-interim (Dee et al. 2011), which were discretized at 37 pressure levels and 1° of latitude and longitude. Note that the geopotential height is used in the reanalysis data, a procedure of properly converting it to the geometric height at each vertical level is required (Nafisi et al. 2012; Dousa and Elias 2014; Zus et al. 2014). Then, the meteorological parameters T , rh were interpolated or extrapolated to the earth's surface as needed.

The topography is the same as that in the GPT2w model, which is represented by a resampled 1°-version of ETOPO5 (Lagler et al. 2013). After achieving these parameters, the T_m of each pressure level above the earth’s surface can be computed using the discretized formula of (1) as follows:

$$T_m = \frac{\sum_{i=1}^N \left(\frac{P_i}{T_i} + \frac{P_{i+1}}{T_{i+1}} \right) \frac{\Delta z_i}{2}}{\sum_{i=1}^N \left(\frac{P_i}{T_i^2} + \frac{P_{i+1}}{T_{i+1}^2} \right) \frac{\Delta z_i}{2}} \tag{4}$$

where i is the i th pressure level, N is the total number of layers, z_i is the thickness of the i th layer.

A linear relationship is found between T_m and height, which can be used to describe the T_m lapse rete (He et al. 2013; Zhang et al. 2017; Chen et al. 2018). The relationship is expressed as follows:

$$T_m = \beta \times h + k \tag{5}$$

where β is the T_m lapse rate in K/km, h refers to the height in km, and k represents a constant. The linear model was utilized to fit the monthly values for T_m lapse rate at each grid point. Taking the T_m and height of each pressure layer at a certain moment into the above equation, we can fit the T_m lapse rate β of the grid point at the corresponding moment.

Considering the distribution of the atmospheric water vapor, the difference between the lower and the upper atmosphere, the vertical adjustments of T_m mostly occur in the lower atmosphere in practical applications. Therefore, we chose three schemes with different height ranges to fit the T_m lapse rate. The range from the surface to a height less than 7 km above the surface is considered as Scheme #1. In Scheme #2 and #3 the ranges decrease to 5 km and 2 km, respectively. The goodness of fit measures, including the coefficient of determination (R -squared) and the root mean square error (RMSE) were adopted to choose the most appropriate scheme.

The processing above yielded 120 monthly values for the T_m lapse rate at each grid point in every scheme. The most appropriate scheme is then used in the next step, namely the time series analysis. We utilized the least-squares adjustment to estimate mean values A_0 as well as annual (A_1, B_1) and semiannual (A_2, B_2) variations for the T_m lapse rate on a regular 1° grid as follows:

$$\begin{aligned} \beta(t) = & A_0 + A_1 \cos \left(\frac{\text{doy}}{365.25} 2\pi \right) + B_1 \sin \left(\frac{\text{doy}}{365.25} 2\pi \right) \\ & + A_2 \cos \left(\frac{\text{doy}}{365.25} 4\pi \right) + B_2 \sin \left(\frac{\text{doy}}{365.25} 4\pi \right) \end{aligned} \tag{6}$$

where doy is the day of the year. The estimated values for each grid point were stored in the gridded input file of the GPT2wh model. For the future calculation of T_m using the

GPT2wh model, the estimated T_m lapse rate can be used to the vertical adjustment of the T_m .

Analysis of the gridded T_m lapse rate

To choose the best height range from the three schemes, we evaluated the fitted results. In Table 1, the globally mean R -squared and RMSEs of the fit in different schemes at all grid points are summarized. The values within square brackets are the minimum and maximum, the first % column is the percentage of those global grids with a value of R -squared < 0.9, and the second % column is the percentage of those global grids with a value of RMSE < 0.5 K. Although the three schemes all achieved a good mean R -squared with a value > 0.98, poor results exist in Scheme #1 and #2, in which the minimum of R -squared are 0.79 and 0.59, respectively. For Scheme #3, only 4 grid points (the corresponding % is 0.006%) have a R -squared value less than 0.9, while the percentages reach up to 0.73% and 5.5% for Scheme #2 and #1, respectively. One can also find from the RMSEs that Scheme #3 significantly outperforms the other two schemes in terms of the mean value, the minimum and maximum, as well as the percentage.

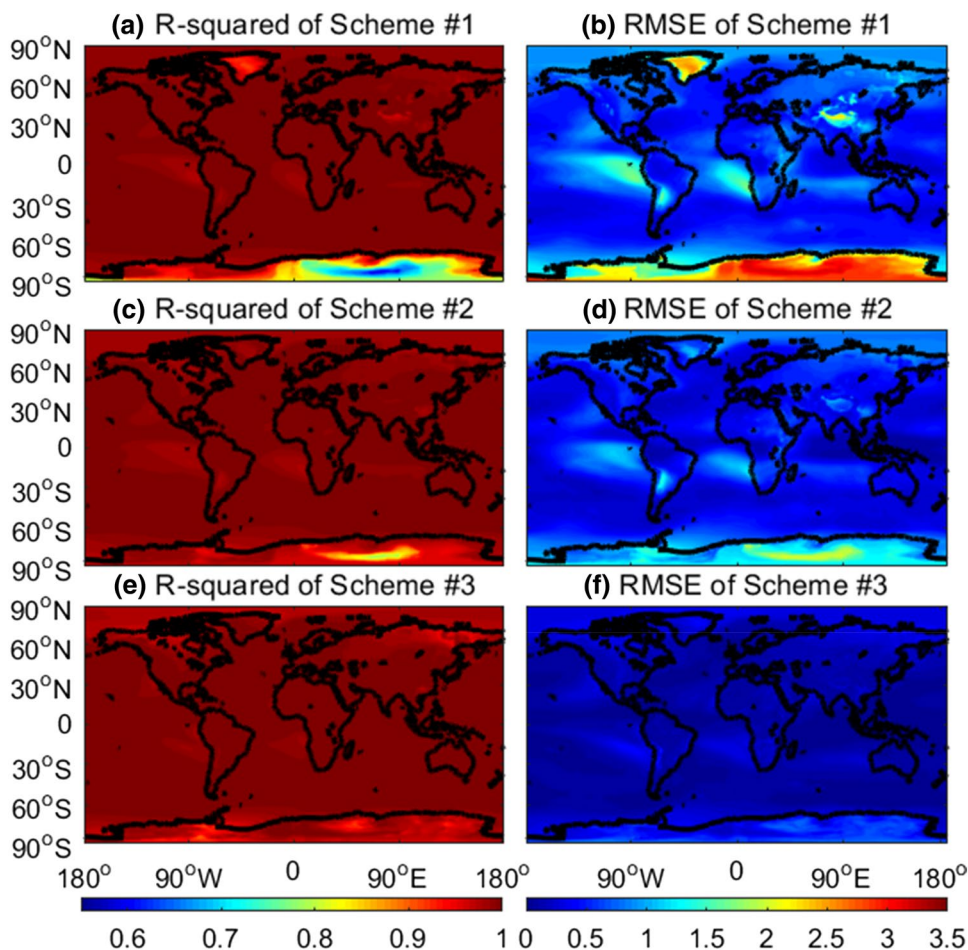
Figure 1 illustrates the distribution of the R -squared and RMSE (not the mean value of all grid points) in different schemes. The fitting results of Scheme #1 show land-sea and regional differences exist in the figure, and poor accuracy appears in some areas, especially in the Antarctic region. The results of Scheme #2 have a significant improvement, but the fit differences between grid points worldwide can still be seen clearly. For example, both R -squared and RMSE have large variations, the range of which is from 0.79 to 0.9998 for R -squared and from 0.08 to 2.12 K for RMSE. Scheme #3 improves the fitting results globally, showing the R -squared greater than 0.9 and the RMSE less than 1.0 K at almost all grid points. Specifically, the RMSE values of Scheme #3 range from 0.02 to 0.86 K, outperforming the other two schemes with a global average RMSE of only 0.17 K and an approximately 62.9% improvement over the worst scheme.

According to the above analysis, Scheme #3, namely the range from the surface to a height less than 2 km above the surface, was selected as the best choice to estimate the

Table 1 Globally mean R -squared and RMSEs of the fit in different schemes

	R -squared	%	RMSE	%
Scheme #1	0.9829 [0.59, 0.9996]	5.5	0.83 [0.22, 3.39]	31.8
Scheme #2	0.9919 [0.79, 0.9998]	0.73	0.53 [0.08, 2.12]	57.4
Scheme #3	0.9926 [0.89, 0.9999]	0.006	0.17 [0.02, 0.86]	94.7

Fig. 1 Global distribution of the *R*-squared (left panel) and RMSE (right panel) in different schemes



mean values as well as an annual and semiannual variation for the T_m lapse rate. Note that the vertical adjustment of meteorological parameters mostly occurs within this range. Therefore, the choice meets the practical application. Figure 2 illustrates the mean values of the T_m lapse rate, its annual and semiannual amplitudes, and the standard deviations of the residuals as estimated by the least square adjustment. The distribution of the mean values is mostly latitude-dependent and altitude-dependent, significantly small absolute values appear at the poles and large absolute values appear at alpine areas, such as the Himalayas, the Andes, and the Rocky Mountains. Annual amplitudes of the T_m lapse rate are strongest at latitudes between 40° N to 70° N (e.g., the amplitudes in north-east Asian and some parts of Canada exceed 1.8 K/km). In addition to the Antarctic region, the semiannual amplitudes of the T_m lapse rate are also evident in northern India, the western Sahel zone, and north-east China. Figure 2d shows that the standard deviation of the residuals of the least square adjustment is less than 0.85 K/km on a global scale, with an average of 0.33 K/km. Overall, Fig. 2 clearly demonstrates that it is not enough to apply a constant lapse rate for the T_m , neither in space nor in time.

Validation of T_m lapse rate

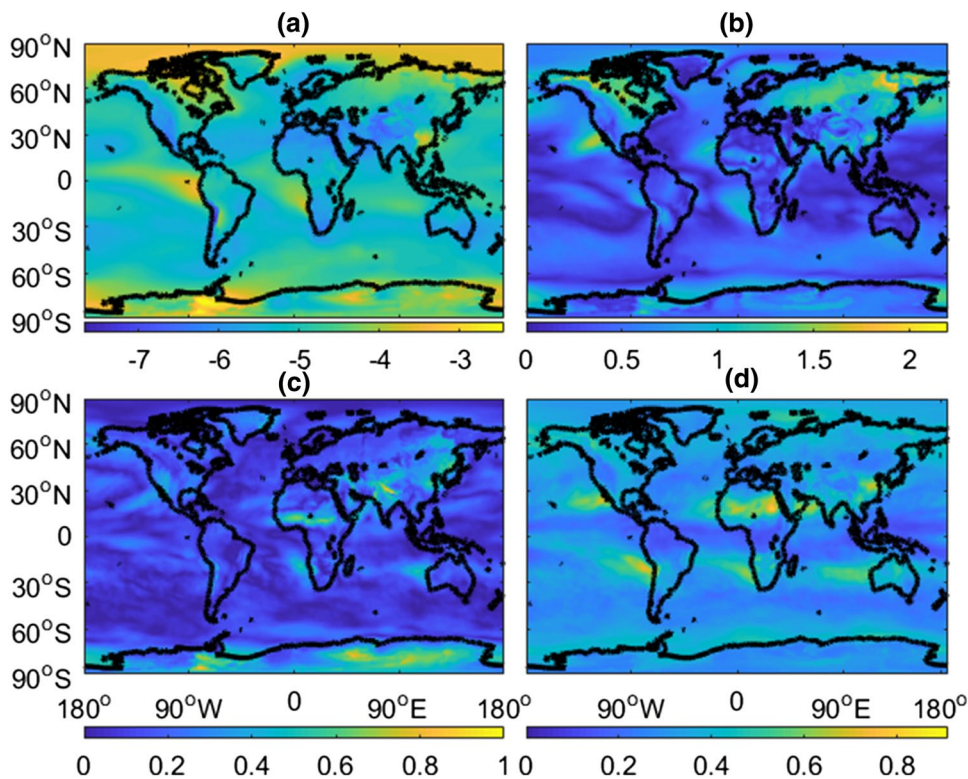
The gridded T_m lapse rate estimated above was added into the GPT2w model, making it a new model called GPT2wh model. To assess the performance of the T_m lapse rate in T_m vertical adjustment, we compared the T_m calculated by the GPT2wh model and the GPT2w model using the reference T_m values derived from ECMWF data and radiosonde data. The two statistical quantities, bias and root mean square error (RMSE), were selected to measure their performance, which can be calculated by the following equations:

$$\text{Bias} = \frac{1}{N} \sum_{i=1}^N (T_m^{C_i} - T_m^i) \tag{7}$$

$$\text{RMSE} = \sqrt{\frac{1}{N} \sum_{i=1}^N (T_m^{C_i} - T_m^i)^2} \tag{8}$$

where $T_m^{C_i}$ and T_m^i are the T_m values from the models and the reference, respectively, and N is the number of the samples.

Fig. 2 Mean values (a), annual amplitudes (b), semiannual amplitudes (c), and standard deviation of the residuals of the least-squares adjustment (d) of the T_m lapse rate



Comparison with ECMWF data

The ECMWF data of 2011 at a resolution of $5^\circ \times 5^\circ$, ranging from 85° N to 85° S in latitude and from 175° W to 175° E in longitude, was used to analyze the reliability of the GPT2wh model for the T_m lapse rate. We collected the meteorological profiles of these 2520 sites at UTC 12:00 each day and computed T_m at different heights for each site to show the T_m vertical adjustment effect of the GPT2wh model. Six height levels were selected as follows: At the earth’s surface (level 1), 300 m higher than the surface (level 2), 600 m higher than the surface (level 3), 900 m higher than the surface (level 4), 1500 m higher than the surface (level 5) and 2000 m higher than the surface (level 6). The T_m data with a temporal resolution of 24 h derived by the ECMWF data were considered as a reference, and the T_m of each site at the same time and same height levels were calculated using the GPT2w and GPT2wh model. Thus, the bias and RMS can be obtained for the two models.

The altitude difference between the site to be computed and the four grid points in the GPT2w model used to interpolate this site directly affects the results of the T_m vertical adjustment using the T_m lapse rate. Thus, Fig. 3 shows the distribution of the altitude differences between the 2520 sites and the corresponding four grid points in the GPT2w model at different height levels. We can see that the altitude differences between the 2520 sites and their four grid points increase with the increasing height levels. The maximum

and minimum altitude difference, as well as the average altitude difference at each height level, is shown in Table 2. The largest altitude difference in all experiments is 2603 m, which appears at level 6, while the smallest altitude difference of 0.1 m appears at level 1. The average altitude difference increases from 54 to 1994 m with the change of height level. Therefore, the height level 6 with an average altitude difference of 1994 m is considered as an experiment with a larger altitude difference, while the height level 1 as an experiment with a small altitude difference in this study.

The globally mean biases and RMSEs of the differences between the T_m derived from the two models (the GPT2wh model and the GPT2w model) and the T_m derived from ECMWF data at the 2520 sites are summarized in Table 3. The results of these 6 height levels are included. Table 3 shows that the GPT2wh model significantly outperforms the GPT2w model. The statistical results of the GPT2wh model, including RMSE and biases, are better than those of the GPT2w model at every height level. The mean bias of the GPT2w model varies greatly at different height levels (from 0.31 to 10.16 K), while it is relatively stable and small for the GPT2wh model. As the altitude difference increases, the mean RMSE of the GPT2w model increases significantly, while the GPT2wh model can always obtain T_m results with a relatively small RMSE. It is found that the improvement of T_m by the GPT2wh model is small at the height level with the smallest average altitude difference, e.g., the mean RMSE is reduced by 0.03 K from 2.92 to 2.89 K at height

Fig. 3 Distribution of the altitude differences between the 2520 sites and the corresponding four grid points in GPT2w model at different height levels (unit: m)

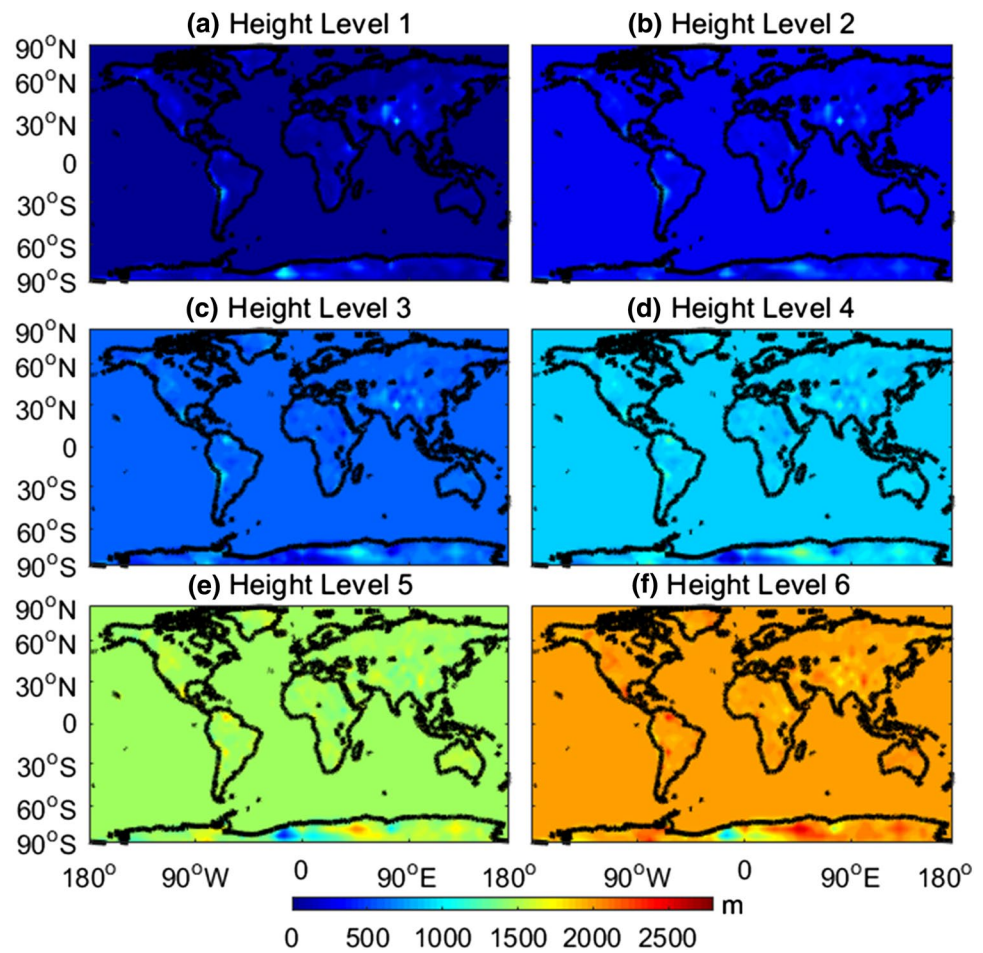


Table 2 Maximum and minimum altitude difference between the 2520 sites and the corresponding four grid points, as well as the average altitude difference at each height level (unit: m)

Altitude difference	Height level					
	Level 1	Level 2	Level 3	Level 4	Level 5	Level 6
Average	54	308	599	896	1495	1994
Maximum	1292	1292	1292	1503	2103	2603
Minimum	0.1	21	48	24	348	848

Table 3 Globally mean biases and RMSEs of the differences between ECMWF-derived and model-derived T_m (in K) on six height levels

Height level	Bias		RMSE	
	GPT2w model	GPT2wh model	GPT2w model	GPT2wh model
1	0.31 [-2.92 3.72]	0.28 [-3.10 2.82]	2.92 [0.95 5.87]	2.89 [0.94 5.65]
2	1.63 [-2.24 5.46]	0.22 [-2.53 3.04]	3.47 [1.31 6.77]	2.96 [0.94 5.87]
3	3.02 [-1.36 7.63]	0.15 [-2.59 3.07]	4.41 [1.85 8.18]	3.04 [0.95 5.91]
4	4.45 [-0.39 9.73]	0.13 [-2.49 3.07]	5.56 [2.95 10.21]	3.11 [0.96 5.92]
5	7.48 [2.08 13.90]	0.27 [-1.91 2.97]	8.26 [3.78 14.27]	3.26 [0.99 6.02]
6	10.16 [4.67 17.22]	0.53 [-1.34 3.12]	10.78 [5.66 17.5]	3.42 [0.99 7.54]

Values within square brackets are the minimum and maximum

level 1, while the improvement becomes apparent in the case of a large altitude difference, such as the improved mean RMSE is 7.36 K from 10.78 to 3.42 K at height level 6.

Moreover, the largest bias and RMSE in the whole experiment appear in the case of the largest altitude difference (height level 6), where these values are 17.22/17.5 K and

3.12/7.54 K for the GPT2w model and the GPT2wh model, respectively. This proves once again that the altitude difference is an important factor in determining the accuracy of the T_m for the two models and is also related to the effect of the T_m vertical adjustment for the GPT2wh model.

Figures 4 and 5 illustrate the global distribution of RMSEs and biases of the differences between ECMWF-derived and model-derived T_m (in K). Only the results of height levels 1 and 6 are given since they represent the cases with the minimum and maximum altitude difference, and the figures of other cases are similar to them. For the GPT2wh model with the T_m vertical adjustment, T_m values with high accuracy can be obtained in any case worldwide. The improvement in T_m accuracy by the GPT2wh model becomes obvious with an increase in the altitude difference from height level 1 to height level 6. At the height level 1, more than 82% and 83% of the sites had RMSE less than 4 K for the GPT2w model and the GPT2wh model, respectively. While at the height level 6, the GPT2w model becomes particularly poor, all the sites had RMSE more than 5.6 K, but for the GPT2wh model, the percentage < 4 K still reaches 67%. For the case of bias, the two models can achieve good T_m results at height level 1, the ranges of bias are from -2.9 to 3.7 K and from -3.1 to 2.8 K for the GPT2w and GPT2wh model, respectively. As the altitude difference increased, the T_m values estimated by the GPT2w model become larger, which results in a big warm bias with the range from 4.7 to 17.7 K at height level 6 while the GPT2wh

model can achieve a good bias result with the range from -1.3 to 3.1 K at this height level.

Comparison with radiosonde data

The GPT2wh model was also evaluated using independent measurements (i.e., radiosonde). A total of 457 globally distributed radiosonde stations that contain available data of over 6 months were selected (Durre et al. 2006). The T_m values of each station at UTC 0:00 and 12:00 every day in 2011 were computed from radiosonde profiles using the integration method and were treated as the reference values to validate the two models.

The statistical results of bias and RMSE for the two models are shown in Fig. 6, in which the spatial variation in the accuracy of these models can be seen. An accuracy of better than 5 K has been achieved at most stations for the GPT2wh model (Fig. 6b), and the percentage reaches 84.2%. While stations with an accuracy better than 5 K account for 75.4% for the GPT2w model (Fig. 6a). The largest improvement is 7.39 K from 11.39 to 4.00 K, and the globally mean RMSE of the GPT2wh model is 3.83 K, which shows approximately 0.33 K (8%) improvement against the GPT2w model. Colors in Fig. 6c, d distinguish two types of stations, one with a warm bias and the other with a cold bias. This is mainly affected by the altitude difference between the radiosonde station and the four grid points. The stations with cold bias always have negative

Fig. 4 Global distribution of RMSEs in the two models tested by using the ECMWF data at height levels 1 and 6 (a, b represent the cases of height level 1 using the GPT2w and GPT2wh model, respectively. c, d represent the cases of height level 6 using the GPT2w and GPT2wh model, respectively. Unit: K)

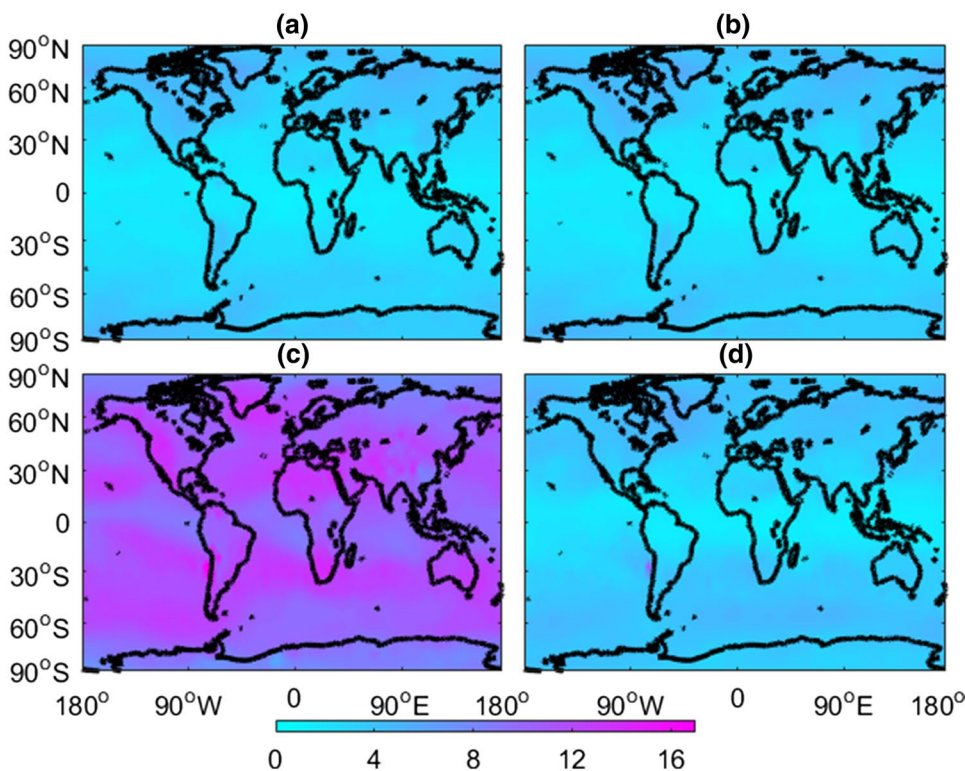


Fig. 5 Global distribution of biases in the two models tested by using the ECMWF data at height levels 1 and 6 (a, b represent the cases of height level 1 using the GPT2w and GPT2wh model, respectively; c, d represent the cases of height level 6 using the GPT2w and GPT2wh model, respectively. Unit: K)

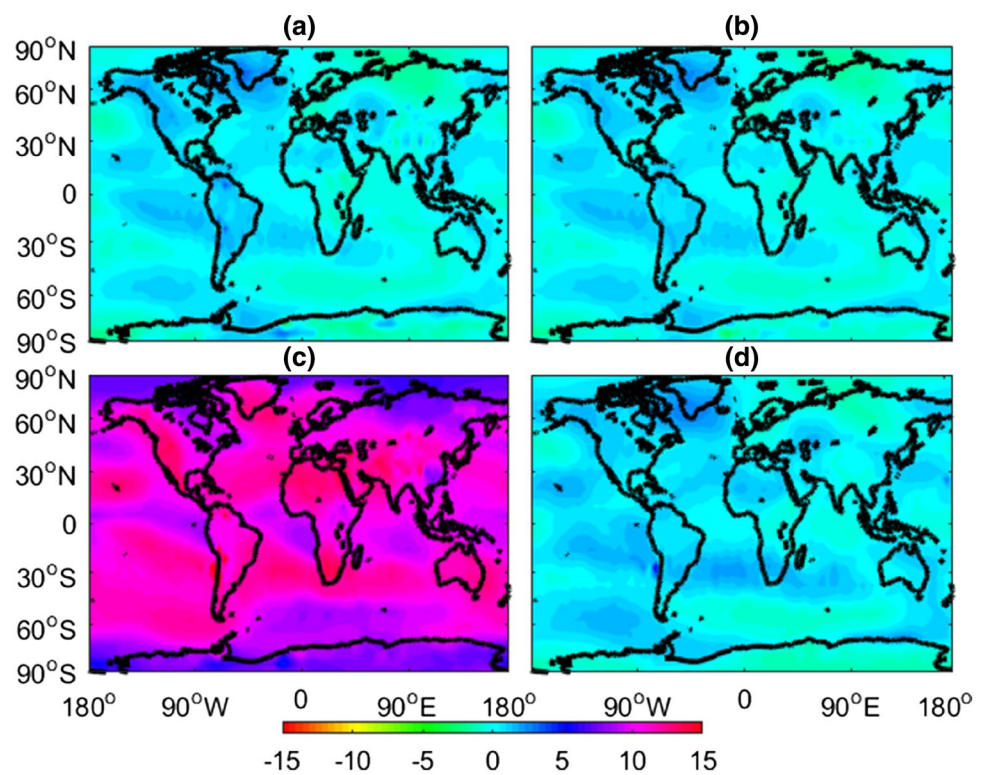
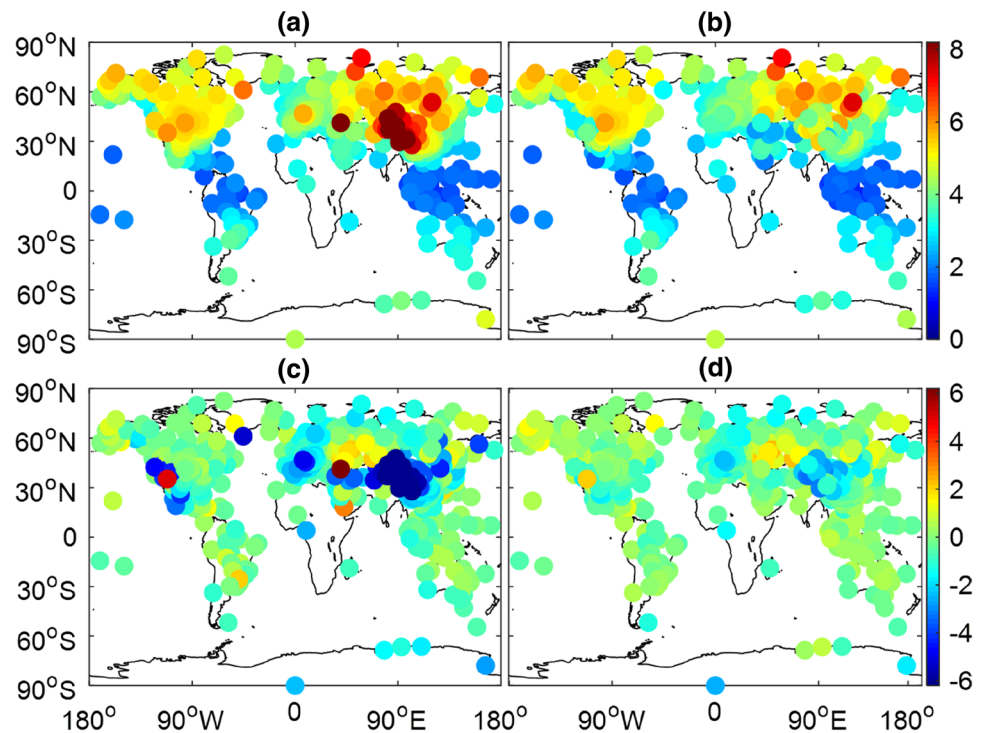


Fig. 6 Global distribution of RMSEs and biases in the two models tested by using the radiosonde data (a, b refer to the RMSEs of the GPT2w and GPT2wh model, respectively; c, d refer to the biases of the GPT2w and GPT2wh model, respectively. Unit: K)



altitude difference, and the warm ones have a positive altitude difference. After the T_m vertical adjustment by the GPT2wh model, the large cold/warm biases of the GPT2w model are obviously reduced. The globally mean biases

are -0.32 K and -0.94 K for the GPT2wh model and the GPT2w model, respectively.

The average altitude differences between the radiosonde stations and the corresponding four grid points of the model

are counted and the change of the RMSE (upper) and bias (bottom) with the altitude difference is plotted in Fig. 7. Both the RMSE and bias of the GPT2w model increase with the increasing altitude difference. While the GPT2wh model can obtain relatively stable RMSE and bias regardless of the altitude difference, it effectively improves the accuracy of the GPT2w model at stations with large altitude differences. According to their altitude difference, the biases and RMSEs of the differences between the T_m derived from

the two models and the T_m calculated from radiosonde data are grouped into four intervals 0–100, 100–200, 200–400 and > 400 m, which are listed in Table 4. As the altitude difference increases, the improvement in the GPT2wh model becomes more apparent, and the values of the improved bias/RMSE are 0.08/0.02, 0.56/0.11, 1.30/0.46 and 3.09/2.61 K, respectively.

The histogram of the T_m residuals, namely the values of subtracting the radiosonde-derived T_m from model-derived T_m , in terms of the mean, standard deviation (SD), median, and mode value, is shown in Fig. 8. All the indicators of the GPT2wh model are better than those of the GPT2w model. The histograms of both the GPT2w model and the GPT2wh model are normally distributed, and the new model is better than the original one with more residuals concentrated around zero. For example, the percentages of residuals in the range of -2 to 2 K are 40% and 44% for the GPT2w and GPT2wh models, respectively.

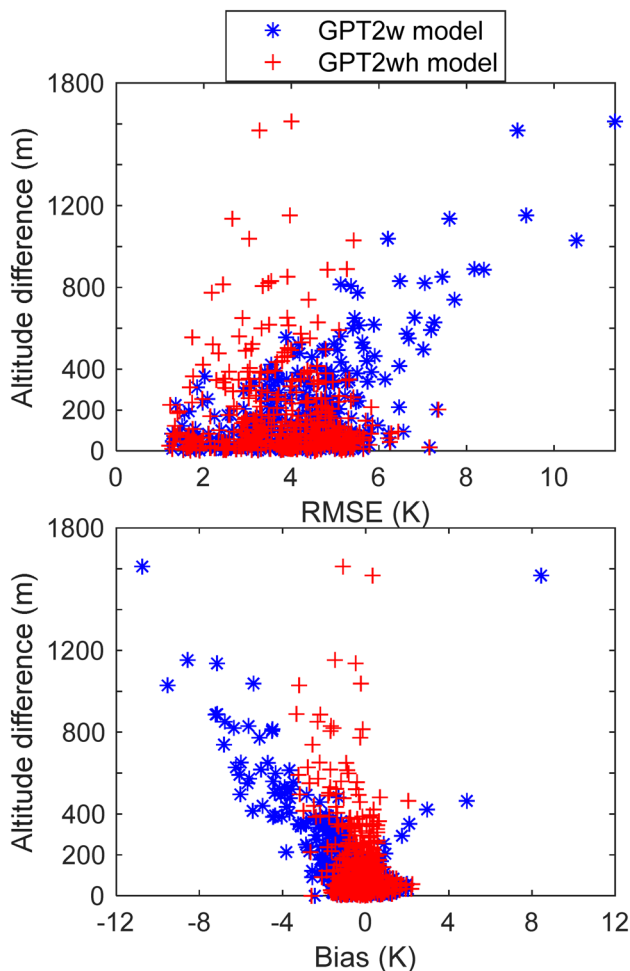


Fig. 7 Change of the RMSE (upper) and bias (bottom) with the altitude difference for the two models

Impact of T_m on GNSS-PWV

In GNSS meteorology, the purpose of determining T_m is to map the zenith wet delay (ZWD) of GNSS signals onto PWV based on the following formula:

$$PWV = \Pi \cdot ZWD = \frac{10^6}{\rho_w R_v (k_3 / T_m + k'_2)} \cdot ZWD \tag{9}$$

where Π is a conversion factor determined by T_m . ρ_w refers to the density of the liquid water; R_v denotes the specific gas constant for water vapor; k_3 and k'_2 are the atmospheric refractivity constants given in Bevis et al. (1994). The ZWD is the zenith wet delay that can be computed by subtracting zenith hydrostatic delay (ZHD) from zenith tropospheric delay (ZTD).

To determine the impact of T_m on GNSS-PWV, we selected the International GNSS Service (IGS) sites with meteorological data recorded and a nearby radiosonde station. Since the IGS can provide accurate ZTD products for each site, the ZHD can be accurately computed by meteorological data based on the Saastamoinen model (1972), and the T_m derived from the nearby radiosonde station is

Table 4 Mean biases and RMSEs of the differences between radiosonde-derived and model-derived T_m (in K) in different intervals

Altitude difference(m)	Bias (K)		RMSE (K)	
	GPT2w model	GPT2wh model	GPT2w model	GPT2wh model
0–100	−0.24 [−2.56 2.03]	−0.16 [−2.51 1.95]	3.89 [1.25 7.16]	3.87 [1.21 7.15]
100–200	−0.77 [−2.58 0.94]	−0.21 [−1.88 0.85]	3.93 [1.50 5.97]	3.82 [1.34 5.85]
200–400	−1.69 [−4.46 2.09]	−0.39 [−2.66 0.64]	4.27 [1.36 6.45]	3.81 [1.23 5.82]
> 400	−4.48 [−10.75 8.44]	−1.39 [−3.33 2.05]	6.22 [3.54 11.39]	3.61 [1.73 5.42]

Values within square brackets are the minimum and maximum

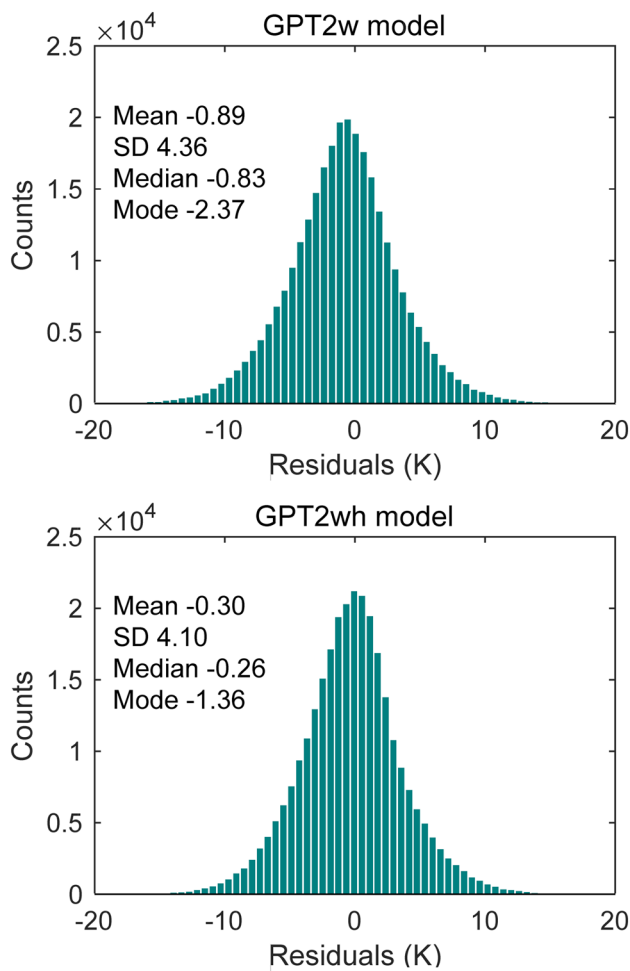


Fig. 8 Histogram of the T_m residuals in 2011 for the two models

regarded as the true value to construct the conversion factor. Based on the above principles, two IGS sites were chosen, one is LHAZ with latitude 29.66° and longitude of 91.10° . The other one is NICO with a latitude of 35.14° and a longitude of 33.40° . The nearby radiosonde stations are Zuls (the station number is 55591) with a distance of 2.5 km from LHAZ and Lcnc (the station number is 17607) with a distance of 1.1 km from NICO, respectively. The average altitude differences between the IGS site and the four grid points are 1031 and 155 m for LHAZ and NICO, respectively. In our experiment, the PWV converted by the radiosonde-computed T_m was treated as a reference value to compare the PWVs converted by the two modeled T_m .

Figure 9 shows the residuals of PWV converted by the two modeled T_m for the two IGS sites in 2011. For the LHAZ site, the PWV residuals of the GPT2w model are negative and improved by the GPT2wh model. This is because the altitude of the LHAZ site is lower than all the four corresponding grid points. This results in the T_m estimated by the GPT2w model being smaller than the radiosonde-computed

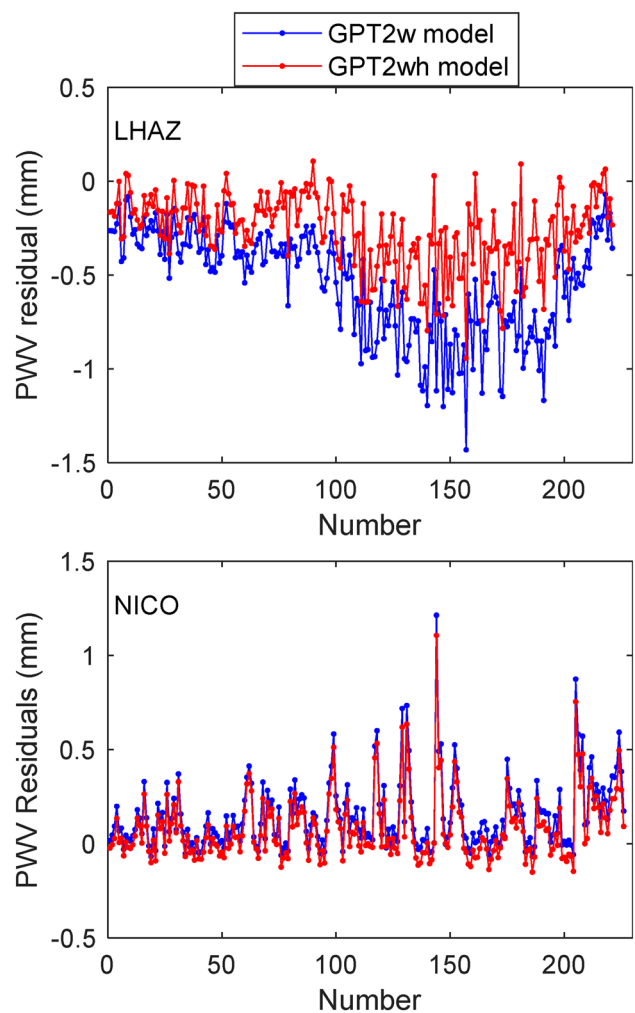


Fig. 9 Residuals of PWV converted by the two modeled T_m for the two IGS sites in 2011

T_m , while the converted PWV is smaller than the true value of PWV. After the vertical adjustment of the GPT2wh model, the value of the estimated T_m and the converted PWV become larger. For the NICO site, the altitude difference between the site and the four grid points is positive. Therefore, most of the PWV residuals of the GPT2w model are positive. In addition, the improvement in the new model at the LHAZ site is more obvious than that at the NICO site. This is due to the LHAZ site (1031 m) having a larger average altitude difference than the NICO site (155 m).

The statistics of the PWV residuals for the two models at the different IGS sites are listed in Table 5. The bias/RMSE are improved by 0.28/0.29 mm and 0.07/0.04 mm at the LHAZ and NICO sites, respectively. This indicates that the improvement in the GPT2wh model on PWV conversion increases with the increasing altitude difference. Moreover, we counted the altitude difference of 507 IGS sites worldwide. The percentage of IGS sites with an altitude difference

Table 5 Biases and RMSEs of the PWV residuals for the two models at different IGS sites

IGS site	Bias (mm)		RMSE (mm)	
	GPT2w model	GPT2wh model	GPT2w model	GPT2wh model
LHAZ	-0.54	-0.26	0.61	0.32
NICO	0.15	0.08	0.23	0.19

larger than 1000 m is 4.1%, the percentage reaches to 12.2% and 56.4% when the altitude difference is set to larger than 500 m and 100 m, respectively. It can be expected that the T_m estimated by the GPT2wh model could effectively improve the accuracy of the PWV conversion at most IGS sites.

Conclusion

The applications of T_m estimated by empirical models is limited because the altitude differences between the GNSS stations and the reference level of the models always exist. Therefore, the T_m vertical adjustment plays a crucial role in obtaining high-precision T_m for the empirical T_m models. The T_m lapse rate along the vertical direction is applied to solve this issue. To adopt a constant as the T_m lapse rate is not sufficient neither in space or in time. Therefore, the development of the GPT2w model, namely the GPT2wh model, was proposed using the 10 years of 37 monthly mean pressure level data from ECMWF. The process of calculating the T_m lapse rate was described in detail. The mean value, as well as annual and semiannual amplitudes for the T_m lapse rate, were determined and analyzed, which is stored in the same format with the other parameters of the GPT2w model.

The comprehensive comparisons between the GPT2w model and the GPT2wh model were conducted using the ECMWF data and the globally distributed radiosonde data. Comparisons with the T_m derived from ECMWF data at 6 height levels show that the altitude difference seriously affects the accuracy of the GPT2w model, and the GPT2wh model can effectively reduce this effect. The statistical results show that the improvement is 7.36 K from 10.78 to 3.42 K at height level 6 and is 0.03 K at height level 1. More than 67% of the sites have an RMSE less than 4 K for the GPT2wh model at each height level, while the percentage is smaller for the GPT2w model. In comparison with the radiosonde data, the mean RMSE and bias values of the GPT2wh model are 3.83 K and -0.32 K, outperforming the GPT2w model with an RMSE and bias of only 4.16 K and -0.94 K, approximately a 8% and 66% improvement over it. Additionally, the impact of T_m on GNSS-PWV was

analyzed, showing that the GPT2wh model can improve the bias and RMSE of the converted PWV at different IGS sites.

The GPT2wh model can improve the accuracy of T_m , especially at the sites which have large altitude differences compared with the GPT2wh grid points and can be used to achieve the T_m at different pressure levels. In further research, the diurnal amplitudes should be explored to improve the situation where the GPT2wh model has little or no improvement in T_m at some epochs. Moreover, the hydrostatic equation should be used to achieve a more robust T_m result.

Acknowledgements Thanks to NOAA, ECMWF and IGS for providing radiosonde data, meteorological reanalysis data and GNSS products. We also thank Böhm for providing the GPT2w model. This study is supported by the National Natural Science Foundation of China (Nos. 41604019 and 41474004). The Chinese Scholarship Council (CSC) has provided the first author a scholarship which allows him to visit the University of Nottingham for one year to research and study in the UK starting November 2018. Acknowledgments are also given to my colleague at the University of Nottingham (Simon Roberts) for the revision to improve the English language and style.

References

- Askne J, Nordius H (1987) Estimation of tropospheric delay for microwaves from surface weather data. *Radio Sci* 22:379–386
- Bevis M, Businger S, Herring T, Rocken C, Anthes R, Ware R (1992) GPS meteorology: remote sensing of atmospheric water vapor using the global positioning system. *J Geophys Res Atmos* 97(D14):15787–15801
- Bevis M, Businger S, Chiswell S, Herring T, Anthes R, Rocken C, Ware R (1994) GPS meteorology: mapping zenith wet delays onto precipitable. *J Appl Meteorol* 33:379–386
- Böhm J, Heinkelmann R, Schuh H (2007) Short note: a global model of pressure and temperature for geodetic applications. *J Geodesy* 81(10):679–683
- Böhm J, Möller G, Schindelegger M, Pain G, Weber R (2015) Development of an improved empirical model for slant delays in the troposphere (GPT2w). *GPS Solut* 19(3):433–441
- Bolton D (1980) The computation of equivalent potential temperature. *Mon Weather Rev* 108:1046–1053
- Chen P, Yao W (2015) GTm_X: A new version global weighted mean temperature model. In: China satellite navigation conference (CSNC) 2015 proceedings II, pp 605–611
- Chen P, Yao W, Zhu X (2014) Realization of global empirical model for mapping zenith wet delays onto precipitable water using NCEP reanalysis data. *Geophys J Int* 198(3):1748–1757
- Chen B, Dai W, Liu Z, Wu L, Kuang C, Ao M (2018) Constructing a precipitable water vapor map from regional GNSS network observations without collocated meteorological data for weather forecasting. *Atmos Meas Tech* 11(9):5153–5166
- Davis J, Herring T, Shapiro I, Rogers A, Elgered G (1985) Geodesy by radio interferometry: effects of atmospheric modeling errors on estimates of baseline length. *Radio Sci* 20:1593–1607
- Dee D et al (2011) The ERA-Interim reanalysis: configuration and performance of the data assimilation system. *Q J R Meteorol Soc* 137:553–597
- Dousa J, Elias M (2014) An improved model for calculating tropospheric wet delay. *Geophys Res Lett* 41:4389–4397

- Durre I, Vose R, Wuertz D (2006) Overview of the integrated global radiosonde archive. *J Clim* 19(1):53–68
- Emardson T, Derks H (2000) On the relation between the wet delay and the integrated precipitable water vapour in the European atmosphere. *Meteorol Appl* 7(1):61–68
- He C, Yao Y, Zhao D, Li K, Qian C (2013) GWM T global atmospheric weighted mean temperature models: development and refinement. In: China satellite navigation conference (CSNC) 2013 proceedings. Springer, Berlin, Heidelberg, pp 487–500
- He C, Wu S, Wang X, Hu A, Wang Q, Zhang K (2017) A new voxel-based model for the determination of atmospheric weighted mean temperature in GPS atmospheric sounding. *Atmos Meas Tech* 10:2045–2060
- Hua Z, Liu L, Liang X (2017) An assessment of GPT2w model and fusion of a troposphere model with in situ data. *Geomat Inf Sci Wuhan Univ* 42(10):1468–1473
- Lagler K, Schindelegger M, Böhm J, Krasna H, Nilsson T (2013) GPT2: empirical slant delay model for radio space geodetic techniques. *Geophys Res Lett* 40(6):1069–1073
- Mendes V, Prates G, Santos L, Langley R (2000) An evaluation of the accuracy of models for the determination of the weighted mean temperature of the atmosphere. In: Proceedings of ION NTM 2000, Institute of Navigation, Anaheim, CA, January 26–28, pp 433–438
- Nafisi V et al (2012) Comparison of ray-tracing packages for troposphere delays. *IEEE Trans Geosci Remote Sens* 50(2):469–480
- Ross R, Rosenfeld S (1997) Estimating mean weighted temperature of the atmosphere for global positioning system applications. *J Geophys Res Atmos* 102:21719–21730
- Saastamoinen J (1972) Atmospheric correction for the troposphere and stratosphere in radio ranging of satellites. *Geophys Monogr Ser* 15:247–251
- Sapucci L (2014) Evaluation of modeling water-vapor-weighted mean tropospheric temperature for GNSS-integrated water vapor estimates in Brazil. *J Appl Meteorol Climatol* 53(3):715–730
- Wang J, Zhang L, Dai A (2005) Global estimates of water-vapor-weighted mean temperature of the atmosphere for GPS applications. *J Geophys Res Atmos* 110:D21101
- Wang X, Zhang K, Wu S, Fan S, Cheng Y (2016) Water vapor-weighted mean temperature and its impact on the determination of precipitable water vapor and its linear trend. *J Geophys Res Atmos* 121:833–852
- Wang X, Zhang K, Wu S, He C, Cheng Y, Li X (2017) Determination of zenith hydrostatic delay and its impact on GNSS-derived integrated water vapor. *Atmos Meas Tech* 10(8):2807–2820
- Yang S, Smith G (1985) Further study on atmospheric lapse rate regimes. *J Atmos Sci* 42:961–966
- Yang F, Guo J, Meng X, Shi J, Zhou L (2019) Establishment and assessment of a new GNSS precipitable water vapor interpolation scheme based on the GPT2w model. *Remote Sens* 11:1127
- Yao Y, Zhu S, Yue S (2012) A globally applicable, season-specific model for estimating the weighted mean temperature of the atmosphere. *J Geodesy* 86:1125–1135
- Yao Y, Zhang B, Yue S, Xu C, Peng W (2013) Global empirical model for mapping zenith wet delays onto precipitable water. *J Geodesy* 87(5):439–448
- Yao Y, Xu C, Zhang B, Cao N (2014) GTm-III: a new global empirical model for mapping zenith wet delays onto precipitable water vapour. *Geophys J Int* 197(1):202–212
- Zhang H, Yuan Y, Li W, Ou J, Li Y, Zhang B (2017) GPS PPP-derived precipitable water vapor retrieval based on T_m/P_s from multiple

sources of meteorological data sets in China. *J Geophys Res Atmos* 122:4165–4183

Zus F, Dick G, Douša J, Heise S, Wickert J (2014) The rapid and precise computation of GPS slant total delays and mapping factors utilizing a numerical weather model. *Radio Sci* 49:207–216

Publisher's Note Springer Nature remains neutral with regard to jurisdictional claims in published maps and institutional affiliations.



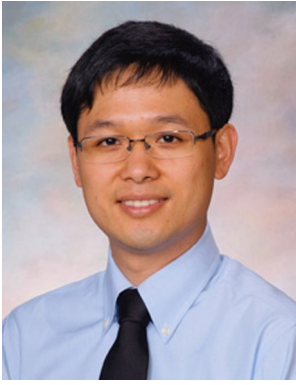
Fei Yang is currently working toward the Ph.D. degree in geodesy and surveying engineering in the school of Geodesy and Geomatics, Wuhan University, Wuhan, China. His main research interests include GNSS meteorology and troposphere tomography.



Jiming Guo received the Ph.D. degree in geodesy and geomatics from Wuhan University, China, in 2001. He is currently a Professor at Wuhan University. His research interests include geodetic data processing, high-precision GNSS positioning technique and applications.



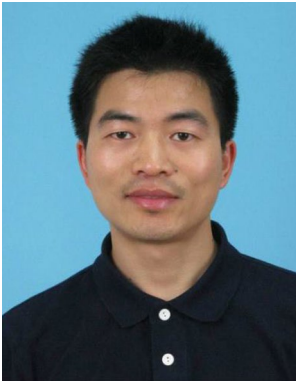
Xiaolin Meng is a professor of Geodesy and Navigation at Nottingham Geospatial Institute (NGI), the University of Nottingham, UK. He received his Ph.D. degrees from Tongji University and the University of Nottingham in 1998 and 2002, respectively. His current research mainly includes large infrastructure monitoring, ubiquitous positioning, intelligent transportation systems and services, GNSS network RTK positioning and quality issues.



Junbo Shi received the Ph.D. degree in geomatics engineering from The University of Calgary, Canada, in 2012. He is currently an associate professor at Wuhan University. His research interests include geomatics data processing, high-precision Global Navigation Satellite System (GNSS) positioning, GNSS-based troposphere/ionosphere modeling and GNSS meteorology.



Yinzhi Zhao is currently working toward the Ph.D. degree in geodesy and surveying engineering in the school of Geodesy and Geomatics, Wuhan University, Wuhan, China. His main research interest is GNSS data processing and Indoor Positioning.



Di Zhang received a Doctor's degree in geodesy and geomatics from Wuhan University, China, in 2017. He is currently working in geodesy and surveying engineering in the school of geodesy and geomatics, Wuhan University, China. His main research interests include GNSS tropospheric zenith delay model and mapping function.